Growing Diamonds in the Laboratory to investigate Growth, Dissolution, and Inclusions Formation processes

Hélène Bureau, Imène Estève, Caroline Raepsaet, Geeth Manthilake

Growing Diamonds in the Laboratory to investigate Growth, Dissolution, and Inclusions Formation processes

Hélène Bureau[1*], Imène Estève[1], Caroline Raepsaet[2], Geeth Manthilake[3]

[1]IMPMC, Sorbonne Université, CNRS UMR 7590, MNHN, IRD UR 206, 4 place Jussieu, 75252 Paris Cedex 05, France

[2] Université Paris-Saclay, CEA, CNRS, SPEC, 91191, Gif-sur-Yvette, France

[3] Laboratoire Magmas et Volcans, Université Blaise Pascal - CNRS - IRD, OPGC, Campus Universitaire des Cézeaux, 6 Avenue Blaise Pascal, 63178 Aubière Cedex, France

GCA

https://doi.org/10.1016/j.gca.2023.12.032

Keywords:

Diamond, water, inclusions, growth, dissolution

*corresponding author: helene.bureau@upmc.fr

ABSTRACT

Replicating lithospheric diamonds experimentally helps reveal their histories at depth, which may be complicated by successive growth and dissolution episodes. Here, we present diamond growth and dissolution experiments to constrain the conditions of diamond formation and residence in the Earth's lithosphere before their transport to the surface. Experiments were performed on mixtures of carbonates, natural lherzolite or MORB, water, diamond seeds, and with or without graphite using multi-anvil presses over a few hours to more than a day at conditions relevant to the lithosphere (7 GPa, 1300–1670 °C). We observed growth within a volatile-rich melt resulting from the miscibility of silicate-carbonate melt and aqueous fluid via the reaction: Carbonate minerals + Silicate minerals/glasses + H_2O = [volatile-rich melt] ± minerals + $C_{diamond}$ + O_2. In the absence of graphite, we observed diamond dissolution within the same hydrous-carbonate-silicate-bearing melts and under similar pressure and temperature conditions used to grow diamond, indicating that diamond formation requires an oxygen sink (graphite, metallic and/or sulphide melts). In dissolution experiments, we also observed resorption features similar to those described in lithospheric monocrystalline diamonds, which we thus attribute to mantle fluids and not to kimberlite-induced resorption during magma ascent. We show that dissolution and growth may alternate in the mantle, and that protracted periods are not necessary to explain natural diamond histories. During experimental growth, inclusions were trapped in diamonds as they are in nature. We observed both syngenetic (formed during growth, representing the parental fluid) and protogenetic inclusions (here particles from the capsule), indicating that both kinds of inclusions can be trapped within a single growth event. Our experiments confirm that inclusions trapped in natural diamonds do not necessarily represent remnants of their parental fluids and are not necessarily contemporaneous: two inclusions near each other within a single monocrystalline diamond may have different histories, and inclusions must be shown to have achieved chemical and isotopic equilibrium before being considered synchronous.

1.Introduction

In 1964, Harrison and Tolansky described the complex structure of an octahedral diamond, which indicates that significant dissolution and regrowth mechanisms occurred successively, a

process since observed in many diamonds (e.g., Smit et al., 2016; Gress et al., 2018; Fedortchouk, 2019; Harris et al., 2022).

In the first lines of their 1964 article, Harrison and Tolansky also asked key questions about diamond growth: whether they grow from solution or from a melt, and whether they represent transformed graphite. Although diamonds most likely grow from fluids, and in the following we will call a fluid "any phase that can flow", through a metasomatic process (Navon et al., 1988), questions remain about the nature of the fluids: melt (dry or volatile-rich), aqueous solutions, supercritical fluids. Numerous attempts have been made to characterize such mantle fluids by studying fluid inclusions trapped in natural diamonds (e.g., Navon et al., 1988; Weiss et al., 2009, 2015, 2022; Nimis et al., 2016; Klein-BenDavid et al., 2004, 2010; Jablon and Navon, 2016), by growing diamonds in the laboratory at mantle pressure (*P*) and temperature (*T*) conditions (Pal'yanov et al., 1999, 2013, 2022; Sokol and Pal'yanov, 2008; Pal'yanov and Sokol, 2009; Bureau et al., 2012, 2016, 2018), or by modelling diamond growth from fluids (e.g., Sverjensky et al., 2015; Huang and Sverjensky, 2020; Mikhail et al., 2021; Rinaldi et al., 2023). It appears that worldwide lithospheric diamonds, whether monocrystalline, fibrous, coated (monocrystalline core and fibrous rim), or polycrystalline, grow from CHO-rich supercritical fluids comprising silicate, water, carbonate, and halogens (Jacob et al., 2014; Bureau et al., 2016; Jablon and Navon, 2016). However, depending on the context (i.e., peridotitic mantle or subduction zones, depth in the mantle, and redox conditions), fluids may differ in their nature and composition (Sokol et al., 2009, 2017; Pal'yanov et al., 2013; Stachel et al., 2017) between endmembers, whether aqueous (possibly saline) or melt (carbonate or silicate) in the case of lithospheric diamonds.The parental fluids may vary within a single diamond (Weiss et al., 2022). Among several examples, fibrous diamonds from Diavik exhibit compositional and isotopic ranges of fluid inclusion compositions (assumed to represent the parental fluid) in concentric layers, evidencing their complex growth from successive batches of fluids (Klein-BenDavid et al., 2004). Furthermore, isotopic profiles (i.e. $\delta^{13}C$, $\delta^{15}N$) are common within single diamonds (e.g., Boyd et al., 1994), indicating that diamond growth can occur in several stages.

Resorption features have been described in most natural monocrystalline and fibrous diamonds based on their surface morphologies (Fetdorchouk, 2019; Harris et al., 2022), cathodoluminescence (CL) imaging (Robinson, 1979; Smit et al., 2016; Smart et al., 2016; Gress et al., 2018; Fetdorchouk, 2019), and isotopic profiles. Resorption was long believed to result from interactions between the host diamond and kimberlitic or lamproitic melts during

magma ascent (Robinson, 1979). However, based on the observed range of resorption morphologies, it was recently shown that if dissolution occurs in kimberlite magmas (Fetdorchouk et al., 2017), it can also occur in the mantle at depth in association with metasomatic events (Gurney et al., 2004; Fetdorchouk et al., 2019). This assumption was confirmed by high pressure and high temperature experiments mimicking diamond resorption in mantle fluids and devoted to decrypting diamond histories from their surface features (e.g., Khokhryakov and Pal'yanov, 2010, 2015; Fetdorchouk et al., 2019).

Monocrystalline diamonds worldwide contain rare silicate mineral inclusions, i.e., true encapsulated pockets of the mantle. However, the significance of these inclusions may differ: do they form contemporaneously with the diamonds and from the same parental fluid (syngenetic) or are they pre-existing, becoming passively trapped (protogenetic)? In some diamonds, inclusions of sulphides, olivines, pyroxenes, and garnets were shown to be protogenetic (Thomassot et al., 2009; Nestola et al., 2017, 2019) based on either stable isotope geochemistry or comparison of the crystallographic orientations of the inclusions relative to those of their host diamonds. It was proposed that included immiscible sulphide phases become isolated from further isotopic exchange upon encapsulation (e.g. Pearson et al., 1998), thus recording the time of their encapsulation (termed later "synchronous"; Nestola et al., 2017). Although the utility of mineral inclusions for dating diamond crystallization is still being investigated, several individual growth-events were identified from populations of inclusions trapped within a single diamond (Koornneef et al., 2017; Gress et al., 2021); these events may have been separated by billions of years, although their duration and frequency remain unknown. The challenges of determining the time of diamond crystallization were well detailed in a recent review (Smit et al., 2022).

To fully utilize the information recorded in diamonds, three processes must be entirely understood: (1) diamond growth in the lithosphere (and in the transition zone and lower mantle); (2) diamond dissolution and the duality between dissolution and growth (i.e., when and how both processes operate in the mantle); and (3) the trapping of silicate and fluid inclusions in diamonds.

Replicating diamonds with inclusions similar to those in natural diamonds is a reliable tool to better understand diamond formation processes.. Here, we grew diamonds in natural lithospheric mantle melts, trapping inclusions of various natures. We show that diamonds may grow and dissolve within the same type of parental fluid over very short times. We suggest

that several successive processes during diamond's histories at depth may make it very difficult to interpret observations of natural diamonds.

2. Materials and methods

2.1 Starting materials

Powders and glasses of different compositions were employed as starting materials (Table 1): a silicate endmember, carbon sources, diamond seeds, and pure water. For the silicate endmembers, we used two natural powders and one glass. The powders were ground from a natural mid-ocean ridge basalt (MORB) from the Indian Ocean and a natural lherzolite from the Lherz massif (Lorand et al., 2008). The glass was prepared using a laser levitation system to obtain a glass of peridotitic composition and free of crystal nuclei. A portion of the natural lherzolite powder was compacted using a hydraulic press, and the resulting pellet was cut into millimetre-sized pieces that were then levitated in a mixed Argon + H_2 gas flux and melted with an Argon laser at 2500–3000 °C for a few seconds; when the laser was stopped, the levitated silicate melt sphere instantaneously quenched into a glassy sphere. Carbonate endmembers were prepared as mixtures of high-purity synthetic $CaCO_3$, Na_2CO_3 and K_2CO_3 powders, and graphite was added to growth experiments (Sigma-Aldrich®). We oxidized commercial diamond seeds (Microdiamant® synthetic monocrystalline 40–60 µm powder) in a furnace at 1000 °C for 10 minutes to form cavities in their surfaces to favour the formation of inclusions. Furthermore, we added 200-500 µm cubic pieces of broken, gem-quality, monocrystalline type-Ia diamond anvil diamonds (Almax-EasyLab®) to some experiments (Fig. 1A). We loaded roughly equal weights of carbonate, water, and either lherzolite powder, a lherzolite glass sphere (half of the growth experiments, Fig. 1C), or MORB powder (two dissolution experiments) into Pt capsules, as well as various amounts of graphite (growth experiments) and diamond seeds (Fig. 1B) or broken pieces (Fig. 1A); for each experiment, all components were carefully weighed and are presented in the Supplementary Table S1. The capsules were carefully sealed by arc welding to avoid any fluid loss, and after each run, the presence of fluid was checked when opening the capsule. All experiments were saturated with respect to carbon, as indicated by the presence of carbonates and graphite (as round globules or bulk masses, only in growth experiments) in the reaction products.

2.2 High-pressure experiments

Experiments were performed in multi-anvil presses at Bayerisches Geoinstitut, Bayreuth, Germany, and at Laboratoire Magmas et Volcans, Clermont-Ferrand, France, as detailed in our previous studies (see Bureau et al., 2012) and summarized here. The high-pressure assembly comprised a 18-mm edge-length MgO octahedron, in which capsules (2×2 mm^2 in size) were introduced, together with tungsten carbide anvils with 11-mm edge truncations (Keppler and Frost, 2005). Graphite heaters were used and temperatures were measured using W(3%Re)–W(25%Re) thermocouples. The experiments were performed at 7 GPa following the calibration curves of the presses, at 1350–1670 °C, and run durations ranging from 4 to 27 hours. We selected temperatures above those expected for lithospheric diamond growth (≥1100 °C) to accelerate experimental processes because of limited access to the multi-anvil presses. We showed that growth kinetics are slower at lower temperatures. In an earlier study, one similar experiment was performed at 1200°C for 7 days, diamond growth on seeds was observed with SEM (Bureau et al., 2012). It shows that slightly increasing the temperature of 100-150°C does not modify the growth process but increases its kinetics.. After quenching to room temperature, the samples were recovered after slow decompression. Capsules were weighed before and after opening to check for the presence of aqueous fluids, and were opened carefully (Fig. 1D) to observe if water leaked out.

2.3 Focused ion beam milling and scanning electron microscopy

The quenched solid products were carefully peaked and gently deposited on stubs covered with carbon tape and studied by Scanning Electron Microscopy (SEM) using a Zeiss Crossbeam Neon40 at Institut de Minéralogie, de Physique des Matériaux et de Cosmochimie (IMPMC, Paris, France). Due to the small sizes of the seed crystals (<50 µm), they could not be separated from the surrounding solid matrix. The interiors of some diamond seeds were exposed by Focus Ion Beam (FIB) milling using a gallium beam on a Zeiss Crossbeam Neon40 at IMPMC. When an exposed seed exhibited an inclusion, it was cut on the other face to obtain a thin section (3–5 µm thick) that was then deposited on a silicon wafer for further analysis (Bureau et al., 2018).

Quantitative chemical analyses of the samples were performed by energy-dispersive X-ray spectroscopy (EDX) in conjunction with either SEM or FIB. The detector was calibrated with a pure copper target at the beginning of each session to determine the beam current. EDX

186 analyses were calibrated using international ASTIMEX® standards for spectral deconvolution
187 and quantification. The resulting precision on the chemical analyses was about 1 wt.%. Strong
188 carbon contributions from the host diamonds, especially in the case of inclusions, were
189 difficult to avoid and quantify.

190

191 **3. Results**

192 ***3.1 Diamond Growth experiments***

193 Our first set of experiments (#50–55; 7 GPa, 1400–1673 °C, 6–24 hours) was designed to
194 grow diamonds in complex fluids (Fig. 2, Table 2a). We used natural lherzolite (powder or
195 glass) as the silicate endmember, synthetic carbonates, synthetic graphite, diamond seeds
196 (powder and/or type-Ia diamond shards), and pure water, with equivalent proportions of fluid
197 (water) and melt (silicates and carbonates). The starting mixtures were inspired by the
198 compositions of micro-inclusions trapped in fibrous diamonds (metal oxides, water,
199 carbonate; Navon et al., 1988) and have been successfully applied in our previous studies
200 (Bureau et al., 2012, 2016, 2018), in which we showed that all diamonds (i.e.,
201 monocrystalline, fibrous, polycrystalline) can grow from these mixtures. We also included
202 experiment #210 from Bureau et al. (2016), in which the silicate endmember was a basaltic
203 MORB glass from the Indian ridge and the carbonate was a natural $CaCO_3$ from the Indian
204 ridge seafloor (7 GPa, 1350 °C, 6 hours).

205 Once quenched, the capsules were pierced, checked for water leaks, and the solid products
206 were deposited on stubs covered with carbon tape. Samples included carbonates, pieces of
207 glasses, graphite agglomerates, and seeds. In all experiments and at all temperatures, we
208 observed diamond growth in the presence of water, either on seeds (Fig. 2A, B, D, F) or
209 spontaneously (Fig. 2C, E). Further images and descriptions of growths are presented in
210 Figures S1 to S5. Growth was more significant in longer duration runs or at higher
211 temperatures (>1600 °C), in agreement with our previous studies (Bureau et al., 2012, 2016).
212 Indeed, massive growth was observed in experiment #52 (Fig. 2B; performed at 1670 °C for 6
213 hours), in which spontaneously grown diamonds attached to the starting seed, which was also
214 growing (Fig 2B). In experiment #53 (1400 °C, 24 hours; Fig. 2D), large rims grew on the
215 starting cubes, explaining the cubic shape. Growth on cubes was also observed in sample #55
216 (1400 °C, 6 hours; Fig. 2F). Spontaneous growth in the matrix was observed as small
217 octahedral diamonds that grew to up to 8 µm during 6 hours at 1670 °C (Fig. S5).

The nature of the carbonate in the lherzolite (K_2CO_3 in run #51; Na_2CO_3 in runs #50 and #55; $CaCO_3$ in run #52; mixtures of all three in runs #53 and #54) and MORB experiments (natural calcite in run #210) did not significantly impact diamond growth, which was of the same magnitude at equivalent pressures, temperatures, and durations (Fig. 2). Compared with previous studies employing different starting silicate materials (synthetic Fe-free, Mg-rich silicate, natural MORB; Bureau et al., 2012, 2016), our experiments confirm that the composition of the silicate does not affect diamond growth.

As already mentioned, we only studied the solid portions of the samples. The solid matrix associated with the diamond seeds (or cubic anvil pieces) mostly comprised chemically heterogeneous materials (Table 3), and no silicate crystals were observed, only silicate glasses. The silicate glasses exhibit a large range of carbon concentrations (Fig. 3A, B, Table 3, sample #52)) and were associated with tiny carbonate crystals of various compositions depending on the starting carbonates. Carbonate crystals were either free in the matrix or attached to all the diamond seeds (Fig. 2, agglomerated in clusters in Figs. 2C and 3A, B). Small diamonds nucleated within the fluid/melt during the experiments (Fig. 2C, E). In contrast with our previous experiments on other chemical compositions (synthetic, MORB; Bureau et al., 2012, 2016), which produced silicate minerals in addition to glasses and carbonates, the lack of silicates in our present experiments suggests that the experiments were above the liquidus. We do not mean that we are working at conditions where the entire mantle assemblage would be melted, but we propose that melting occurs only locally, where the discrete volumes of metasomatic volatile-rich fluids percolate the solid "dry" mantle and gradually dissolve some minerals from the mantle assemblage around.

In sample #52 (7 GPa, 1670 °C), we observed large areas of highly vesiculated glass with a vermicular texture indicating either the presence of coexisting aqueous fluid (lost upon opening the capsule) and volatile-rich melt at the conditions of the experiment (Fig S1),) or the immiscibility process of a unique very hydrous-rich melt due to quench effect. In one such area, we observed octahedral nano-diamonds (<0.2 µm) *in situ* within the quenched silicate melt (Fig. 3A, B, S1).

EDX analyses evidenced strong carbon contamination in the matrix (Table 3; all carbon concentrations expressed as wt.% CO_2). Iron was not present in the matrix because possibly lost to the Pt capsules during the runs (Grove, 1981) and/or partly dissolved in the aqueous fluid phase. The compositions of the amorphous glassy phases associated with diamond seeds were mixtures of the starting silicate and carbonate compositions (Table 3 and Table S2).

Some diamond seeds exhibiting significant growth were milled with a FIB, and all were found to contain inclusions. Figure 4 exhibits the four milled diamonds (#53-1, #53-6, #52-5, #52-9) that showed the most significant growth. Inclusions were observed to be isolated or along the initial surfaces of the starting seeds (particularly in diamond #53-1; Fig. 4B, Fig S2). We observed inclusions of different types: mixed glasses with vesicles, fluids (i.e., holes corresponding to fluids lost during FIB milling), and massive metal inclusions. No inclusions contained silicate minerals, whether in experiments with lherzolite powder (starting crystals present) or lherzolite glass (starting crystals absent), confirming that the system was above the liquidus. The absence of crystals can also be explained by the rapid quench following equilibration at high pressure (HP) and high temperature (HT). In nature, though, trapped melts in diamonds do crystallize after their emplacement.

The compositions of the glassy inclusions (red crosses in Fig. 4C, F, I, L) are reported in Table 4 (on a volatile-free basis); they were similar to the glassy matrix embedding the diamonds and thus represent the parental fluid. The large metal inclusions were pure platinum (see Fig. 4C and red arrows in Fig. 4B) and were observed together with the glassy/fluid inclusions in several samples, as in our previous studies (Bureau et al., 2012, 2016). These Pt particles were probably either produced as spatter when welding the capsules, or torn from the capsule walls at HP-HT run and trapped as inclusions.

The uniform growth observed around the open seed (FIB milling), presented in Figure 4A recalls coated diamonds with monocrystalline cores surrounded by fibrous rims, but here, inclusions were trapped only at the starting surface of the seed and the overgrowth was monocrystalline. Because this diamond was cut perpendicularly to the growth direction, we were able to estimate that it grew 3–5 µm in 6 hours at 1670 °C, corresponding to a growth rate of 20 µm per day.

3.2 Diamond Dissolution Experiments

Our second set of experiments (#31, #32, #35, #38, #44, #45, #49; 7 GPa, 1300–1450 °C, 5–27 hours), was designed to study diamond dissolution (Fig. 5, Fig. S6 and S7, Table 2b). We used either natural lherzolite (#31, #32, #44, #45, #49) or MORB powders (#35, #38) as the silicate endmembers, together with synthetic carbonates, diamond seeds, pure water, and, in experiments #35, #38, and #49, type-Ia diamond pieces. Graphite was not added to the starting materials.

Growth did not occur in any of these experiments and diamonds exhibited dissolution features, the most representative of which are shown in Figures 5, S6, S7. Resorptions were more or less pronounced depending on the experimental duration. Matrix products were quenched glasses and carbonates, as observed in our growth experiments (see previous subsection).

There were no clear textural differences in seed resorption features between experiments using MORB or lherzolite, suggesting that dissolution did not depend on the composition of the silicate endmember. In our experiments, seeds were partly dissolved (#45, Fig. 5G, Fig S6), exhibit (111) preserved faces (Fig S7), strong trigonal etches at 1350 °C (#44, Fig. 5H) for starting diamond seeds, and etches were cuboctahedral at 1400 °C for starting diamond cubes (#49, Fig. 5I). Resorption was so pronounced that it reached lamination in experiments at 1450 °C (#32, 6 hours, Fig. 5A; #35, 5 hours, Fig. 5B) and graphitization of the seeds after 27 hours at 1300–1400 °C (#38, Fig. 5D).

Large type-Ia diamond pieces (200–500 µm) introduced with the small seeds in experiment #38 also exhibited significant resorption textures (Fig. 5C, E, F); for example, a 200 µm cube was strongly rounded (Fig. 5C). Some diamonds exhibited crystal rounding and stepped surfaces (Fig. 5E) that could have formed either during growth (Sunagawa, 1984) or resorption (Viljoen et al., 1992). We also observed deeply etched cubic pits (Fig. 5F) in large cubes.

In summary, in short-duration experiments, the starting seeds presented trigonal etches and some were laminated, whereas those in the long-duration experiment were transformed into graphite. Large diamond pieces loaded in the short-duration experiments presented cuboctahedral dissolution features, whereas those in the long-duration experiment exhibited a rounded final shape and large cubic pits, with surfaces so etched that they became stepped.

4. Discussion

4.1 Diamond growth versus dissolution in the mantle

Diamond growth occurred in all growth experiments, which contained lherzolite + carbonate (Ca, Na, K, or a mixture) + water + graphite, as is the case when the silicate is iron-free (Bureau et al., 2012) or MORB (Bureau et al., 2016). At the highest temperatures (1670 °C, experiments #52 and #50), a single fluid must be present; it may be either a supercritical fluid

or a hydrous super-solidus melt. This was evidenced by the vermicular nature of the glassy quench phase (Fig. 3), suggesting that immiscibility or unmixing due to strong water degassing developed , as observed *in situ* in diamond anvil cell experiments (Bureau and Keppler, 1999), where aqueous fluid and hydrous melt are formed during quenching. Furthermore, inclusions trapped in the diamonds during growth (Fig. 4) contained both glass and void space, which was originally filled by an aqueous fluid before the inclusion was intersected during milling. In run #52 (1670 °C, 7 GPa), nano-diamonds embedded in the glassy layer (Fig. 3) indicate that diamonds nucleated within a hydrous melt. At lower temperatures around 1400 °C, two fluid phases may have been present: a silicate/carbonate melt and a (solute-rich) aqueous fluid. These results are in good agreement with phase diagrams (Wyllie and Ryabchikov, 2000; Dvir and Kessel 2017) showing that at our higher-temperature conditions (7 GPa, 1430–1670 °C), the system lherzolite-CO_2-H_2O is above both the solidus and possibly a critical point. According to Wyllie and Ryabchikov (2000), the minimum depth of the critical point can be constrained from diamonds to 125 km, but there is no constraint on the maximum depth. At depths beyond the critical point, solid peridotite co-exists with supercritical fluids varying continuously in composition (Fig. 6, Tables 3 and 4), in agreement with natural observations (e.g., Klein-BenDavid et al., 2004; Weiss et al., 2015).

Figure 6 shows that part of the compositions of inclusions and matrix glasses in our experiments mirrors that of inclusions trapped in fibrous diamonds, making a trend between silicic endmember and low and high-Mg endmembers (see Fig. S8). We propose that they reflect the discrete metasomatic fluids responsible for diamond growth in the mantle. The range observed between the 3 endmembers recalls recent studies (Mikhail et al., 2021; Rinaldi et al., 2023) proposing that a single fluid may be parent for the formation of eclogitic, websteritic and peridotitic silicate inclusions. The results are consistent with Weiss et al. (2022), who proposed that carbonate-bearing high-density fluids (HDFs) best represent the oxidation state of carbon in diamond-forming fluids, not only for fibrous diamonds, but also for most natural (Jablon and Navon, 2016) monocrystalline diamonds.

The oxidation state of the lithosphere is below the Enstatite + Magnesite = Olivine + Diamond buffer (EMOD), meaning that carbonate-bearing fluids/melts or HDFs would unlikely be the source of most diamonds. Nonetheless, Stagno et al. (2013) showed that pure carbonate melt is stable at more reducing conditions than EMOD. Stachel and Luth (2015) also argued that the buffering capacity of the lithosphere is small, and that an oxidized melt (i.e. HDF) can migrate through and react with the reduced lithosphere to form diamonds.

Two major reactions that are applicable to nature could describe diamond growth in our experiments:

$$\text{Carbonate minerals + Silicate minerals/glasses + } H_2O = \text{[volatile-rich melt]} \pm \text{minerals + } C_{diamond} + O_2 \quad (1)$$

or:

$$CO_2 + CH_4 = 2C + 2H_2O\ . \quad (2)$$

Reaction (1) would involve the reduction of either CO_2 or carbonate, and diamond growth would be associated with oxygen consumption. In contrast, reaction (2) is based on carbon oversaturation, and would imply isochemical diamond precipitation and the conservation of oxygen (Deines, 1980; Stachel et al., 2017).

If we assume reaction (2), the oxygen fugacity in the lithospheric mantle would be buffered by the fluid rather than the wall rock. In this scenario, diamond precipitation would occur in the presence of two dominant carbon fluid species (CO_2 and CH_4) co-existing with a water-rich fluid with maximal water content (i.e. almost no methane at EMOD; Stachel et al., 2017). This process has been used to model carbon isotopic fractionation during diamond growth from mixed CH_4- and CO_2-bearing fluids, which generates different results relative to diamond crystallization from a single carbon fluid species. It was successfully applied to match *in situ* observed co-variations of $\delta^{13}C$, $\delta^{15}N$, and N content in peridotitic diamonds from Marange, Zimbabwe (Smit et al., 2016), where CH_4 fluid inclusions were found (Stachel et al., 2017). However, this reaction does not explain why diamonds do not grow when graphite is absent, but instead dissolve.

If we assume reaction (1) (see Bureau et al., 2016), the volatile-rich melt contains C-O-H species, dissolved in silicate melts (H_2O, OH^-, and CO_3^{2-} bonded with cations). This reaction applies for all starting silicate compositions (e.g., lherzolite, MORB, synthetic) and carbonates (Na_2CO_3, K_2CO_3, $CaCO_3$). Carbon can be dissolved in in the hydrous melt, as carbonate groups. In this reaction, the oxygen fugacity would be close to or below EMOD (e.g., Stagno and Frost, 2010). Reaction (1) is therefore consistent with our experimental results.

In previous experiments performed at the same pressure (7 GPa) and using ^{13}C doped starting carbonates and graphite, we used the isotopic composition of diamonds to estimate the isotopic signature of their source and identify it (Bureau et al., 2018). In that study, a few

seeds were milled using a FIB to expose the portions of diamonds that grew during the experiments and trapped inclusions. Among those inclusions, we observed micro-diamonds spontaneously grown in the fluid, then trapped in the seeds within the first few hours of the experiments. We analysed the $\delta^{13}C$ signatures of those micrometric diamond inclusions by nanoSIMS and compared them with the signatures of the starting materials. The diamonds grown in those experiments had similar signatures ($\delta^{13}C = -14.19 \pm 3.1‰$) to those of the starting carbonates ($\delta^{13}C = -11.40 \pm 0.1‰$), evidencing growth at isotopic equilibrium with a carbonate source. Furthermore, the isotopic signatures of those diamonds (−14.19‰) could not have resulted from contamination by the starting diamond seeds because the seeds had isotopic compositions ranging from −30.4 to −23.6‰ (±1.6‰). The signatures of the diamond inclusions trapped in new growths also differed from those of the starting graphite ($\delta^{13}C = -26.35 \pm 0.1‰$), except for diamonds grown at >1600 °C, which had $\delta^{13}C = -27‰$ on average, compatible with graphite dissolution in the fluid. That study demonstrated that below 1600 °C, only carbonates, and not graphite, are dissolved in the fluid, consistent with the recovery of graphite agglomerates after low-temperature experiments (Bureau et al., 2016). In our experiments, the volume of newly formed diamonds is small relative to that of the carbonates, then, since the reaction proceeds by solution and dissolution of carbon in the carbonatitic melt, the isotopic composition of the carbonatite would vary by only a small amount and the new diamond growth would acquire the composition of the carbonatitic melt.

Above 1600 °C, which is not relevant to the growth of natural lithospheric diamonds, graphite dissolves in the fluid and provides carbon for diamond growth. In this case the isotopic composition is different (Bureau et al., 2018).

If reaction (1) applies, because oxygen is produced, another reaction must occur to react with the newly available oxygen. Graphite would act as an oxygen sink, and possibly as a redox buffer:

$$C\ (graphite) + O_2 = CO_2 \quad (3)$$

If reaction (3) does not occur, neither does reaction (1), which can explain why diamonds dissolved when graphite was not included as a starting material in our experiments.

This is a general observation, and we here refer to the recent review of Luth et al. (2022) on diamond growth studies performed using various growth media. In all reported experiments on diamond nucleation and growth in silicate melts using graphite as the unique carbon

source, neither nucleation nor growth has been reported below 1500 °C. In particular, in the experiments of Fagan and Luth (2011), growth was not observed at 1300 or 1500 °C, but did occur above 1500 °C. Furthermore, except for the study of Bataleva et al. (2012), all experiments reporting diamond nucleation and growth in carbonate-silicate systems used graphite as a starting material (Luth et al., 2022). In the study of Bataleva et al. (2012), when no graphite was added to the carbonate and silicate starting materials, growth on seeds occurred at 1550 and 1650 °C in Pt capsules, whereas dissolution was observed at lower temperatures; in contrast, diamond growth occurred at 1350–1450 °C in experiments using Pt-graphite capsules. All reported experiments that grew diamond in multi-component carbonate-silicate media and/or diamond-forming rocks at temperatures relevant to the lithosphere used graphite either as a starting material or a container (capsule). When graphite was not used in either manner, diamond growth was not observed except when iron was present (Litasov et al., 2014), growth occurred by reduction of carbonates from natural carbonate-bearing eclogites concomitant with Fe^{2+} oxidation of garnets (Kiseeva et al., 2013), or under an electric field (diamond growth on a Pt cathode; Palyanov et al., 2021). Another potential diamond source that is relevant to the Earth and has been investigated experimentally is the carbide system; in the review of Luth et al. (2022), all experiments reporting diamond nucleation and growth involved the presence of graphite and/or metal (Fe, Fe_3C) in the starting materials.

This general observation is corroborated by the examination of dissolution experiments; graphite was not added to any of the numerous dissolution experiments reviewed by Luth et al. (2022).

It has been proposed that diamond growth and dissolution might alternate within the same system, depending on carbon saturation and redox conditions (Khokhryakov and Pal'yanov, 2007). In both the growth and dissolution experiments of this present study, the fluids were carbon-saturated, as indicated by the carbon-rich compositions of the matrix products (Table 3). Oxygen fugacity is certainly an important parameter. Palyanov et al. (2013) performed experiments devoted to diamond growth in subduction environments during mantle-slab interactions down to 240 km depth (i.e. at 6 and 7.5 GPa and 1200–1650 °C) in the $Mg_{0.9}Ca_{0.1}CO_3$-Fe^0 and $Mg_{0.9}Ca_{0.1}CO_3$-Fe_3C systems. Within a single carbonate-bearing experimental charge, they observed that diamonds formed both in oxidized Ca-rich carbonate melts and in reduced Fe-C melts, but no dissolution was reported.

The above laboratory experiments reproduce the natural growth or dissolution of diamonds in the lithospheric mantle. Indeed, many natural diamonds evidence alternating dissolution and growth events and/or successive growth events in the mantle, as shown by CL mapping of polished diamond sections and/or isotopic profiles within individual diamonds (e.g., Boyd et al., 1994; Zedgenizov et al., 2014; Smart et al., 2016; Gress et al., 2021). If natural diamond growth involves reaction (1), consistent with our present experiments, it requires the presence of components capable of reacting with the O_2 produced by the reaction. Graphite is a good candidate because it is present as inclusions in many diamonds (e.g., Stachel et al., 2022) and possibly as single crystals (e.g., Glinnemann et al., 2003).

Other oxygen sinks could be metallic phases and/or sulfides: sulfide inclusions (e.g., pyrrhotites) are found in many diamonds (see Stachel et al., 2022), and metallic inclusions are present in natural lithospheric diamonds (e.g., Stachel et al., 1988; Bulanova et al., 1998; Daver et al., 2022). The presence of metallic Fe and Fe_3O_4 inclusions was also inferred from X-Ray absorption spectroscopy and Mössbauer spectroscopy analyses of fibrous diamonds (Shiryaev et al., 2010), confirming that diamond formation can occur over a large range of fO_2 conditions in the lithosphere.

The morphologies of the initial diamond seeds and cubes (Fig. 1) recovered from our dissolution experiments recall those produced in diamond dissolution experiments on water-bearing carbonate melts at 5.7 GPa and 1300 °C during 30–75 hours (Khokhryakov and Palyanov, 2015). The dissolution textures observed in our experiments (Fig. 5) may be due to the presence of silicates, excess H_2O (>10 wt.%), and high H_2O/CO_2 ratios (1.6–7.6, Table 2), where the highest ratios were associated with the appearance of cuboctahedral shapes for starting diamond cubes (Figure 5I); and showing rounded shapes with trigonal pits (Fig. S6) and preserving (111) faces for starting diamond seeds (Fig. S7). Cuboctahedron shape may be considered as the equivalent stage of morphological dissolution for a intially cubic diamond than dodecahedron is for an initially octahedral diamond. The round final shape of the large initial diamond cube in experiment #38 (Fig 5C) occurred at H_2O/CO_2 = 3.2, but over a relatively long duration of 27 hours. The differences observed between dissolution on seeds and dissolution on cubes also relate to the fact that the surfaces of the starting seeds were oxidized, whereas the surfaces of the broken cubes were not (Fig. 5B–F). As expected, temperature also exerted an important control on resorption, because total lamination was observed at 1400 and 1450 °C, but not at 1350 °C.

In their very detailed study, Fedortchouk (2019) combined morphological observations of natural diamonds with descriptions of dissolution and etching experiments. This paper demonstrated the importance of the experimental approach to understanding diamond histories by differentiating resorption that occurred within the mantle source from that which occurred within the kimberlite magma during its ascent to the surface. It is shown that the shape and size of etch pits on diamond surfaces depend on temperature and the H_2O/CO_2 ratio in the fluid, whereas pressure affects the efficiency of diamond crystal-shape transformation from octahedral to rounded, resorbed forms (Fedortchouk, 2019). When the effect of temperature is significant, we observed a change of form at constant pressure (7 GPa), the most significant being the appearance of cuboctahedral shapes in experiment #49 at 1400 °C, also at the highest H_2O/CO_2 ratio (Fig. 5I). The dominant H_2O effect is also shown Fig S7 with the preservation of the (111) faces of the starting seeds (see Fedortchouk, 2019). Compared to the classification scheme for natural diamond resorption morphologies proposed by Fetdorchouk (2019), our results confirm the destructive character of partial H_2O + CO_2-bearing melts. Following their classification, the dissolution morphologies produced in our experiments fit well with mantle resorption and are applicable to natural diamonds.

Our experiments suggest that in nature, a single diamond may record successive growth and dissolution events in similar fluids but under different conditions, in agreement with observations of natural diamonds. These processes may alternate over very short periods of time, as exemplified by our experiments spanning a few hours to a few days. Therefore, protracted episodes of metasomatism between the successive stages are not required to explain observational data from natural diamonds; diamond growth/dissolution in the lithosphere can be rapid. This chimes with recent work predicting the exact same alternation between dissolution and growth during single metasomatic events (Mikhail et al., 2021; Rinaldi et al., 2023). This demonstrates that large portions of the histories of natural diamonds may have been lost during successive, possibly brief, dissolution events.

4.2 Inclusions trapped in diamonds

In our present and previous synthesis experiments, silicates did or did not crystallize depending on the *P-T* conditions, and therefore, when present, syngenetic crystals were trapped as inclusions along with melt (i.e. glass) and/or fluid, or supercritical fluid if the system was beyond total miscibility (Bureau et al., 2016). The high growth rate of synthesized

505 diamonds is the most probable reason for the abundance of entrapped hydrous carbonate-
506 silicate melts and H_2O-CO_2 fluids that represent the diamond-forming media (Bureau et al.,
507 2012, 2016, 2018; Bataleva et al., 2016). It is experimentally shown that all types of diamonds
508 (monocrystalline, fibrous, polycrystalline) can grow in the same media (Bureau et al., 2012,
509 2016). The presence of very thin hydrous silicate films between mineral inclusions and their
510 gem-quality host diamonds (peridotitic or eclogitic) also suggests that the diamond forming
511 medium is composed of water-rich fluids (Nimis et al., 2016). Furthermore, Jablon and Navon
512 (2016) described micro-inclusions trapped along the twinning plane in natural twinned
513 diamonds; the major element compositions of most of these inclusions were similar to those
514 of carbonate-bearing HDFs in fibrous diamonds. They, too, concluded that the mechanism of
515 diamond formation is the same for most diamonds. Therefore, growth kinetics may be a
516 important parameter determining whether a diamond will be monocrystalline or fibrous, with
517 a potential dependence on the presence of water. In natural monocrystalline diamonds,
518 entrapment of the source fluid/melt may not be possible because of the slow growth rates.

519 In our previous study, syngenetic crystals of different compositions were observed as
520 inclusions (phengite, rutile, coesite, carbonates, and diamonds; Bureau et al., 2016), but in our
521 present experiments, no silicate crystals were trapped as inclusions or found within the solid
522 matrix in equilibrium with diamond. Instead, we observed quenched glasses of various
523 compositions between lherzolite and carbonate endmembers (Fig. 4, Table 4). This is likely
524 due to the fast quench rates that surely differ from those experienced by natural diamonds.
525 Whether crystalline or not, these inclusions are syngenetic and represent the diamond
526 crystallization environment.

527 Along with the syngenetic inclusions, we observed pure platinum particles included in a rim
528 in the diamond that corresponds to the initial surface of the diamond seed (this is particularly
529 evident in Fig. 4B, S2). Such inclusions are also observed along with inclusions of fluids,
530 melts, and crystals in a few diamonds grown in previous experiments (Bureau et al., 2012,
531 2016). These particles were from the platinum capsule walls, which could be seen as
532 analogous to the "surrounding rock". Although platinum might provide a diamond nucleation
533 site in long-term experiments on the kimberlite-graphite system (Pal'yanov et al., 2015), we
534 did not observe any diamonds crystallized on the capsule walls, and therefore we suggest that
535 platinum particles were passively trapped in the diamonds as protogenetic inclusions.
536 Although one might argue that they were previously dissolved in the fluid and would
537 therefore represent syngenetic inclusions, this is very unlikely because the solubility of

platinum in silicate melts is on the order of a few tens of ppm (e.g., Blaine et al., 2005; Bezmen et al., 2006).

In most cases, it is shown that inclusions trapped at different locations within a single diamond record either one growth event or successive events separated by long periods of time (e.g., Klein-BenDavid et al., 2004; Bulanova et al., 2014). For example, dating of individual growth zones in diamonds from Orapa, Bostwana, revealed three distinct ages spanning 3 Ga to 0.3 Ga from core to rim (Gress et al., 2021). In such cases, it is generally assumed that inclusions trapped in the different zones are contemporaneous with growth (e.g., Koornneef et al., 2017; Gress et al., 2018, 2021), although they might also be protogenetic (e.g., Thomassot et al., 2009; Nestola et al., 2017, 2019). It has been proposed that, because inclusions are small and diffusive processes are fast at mantle temperatures, pre-existing host-rock minerals trapped as inclusions in diamonds chemically and isotopically equilibrate during fluid-mediated growth events, and are therefore "synchronous" but not necessarily syngenetic (Nestola et al., 2017, Stachel et al., 2022). Thus, the lack of syngeneity does not necessarily preclude inclusion-based diamond dating (Smit et al., 2022). Although believed to be exceptional (Stachel et al., 2022), disequilibrium observed among non-touching inclusions (e.g., Griffin et al., 1988; Bulanova, 1995; Wang, 1998) reflects their incorporation either during growth in chemically evolving environments or in different generations (syngenetic and protogenetic) without achieving chemical and isotopic equilibrium. As a last comment, our data agree with Rinaldi et al. (2023) suggestion based on mineral inclusion compositions trapped in natural diamonds that the paragenetic groups used to classify diamonds should not be considered a genetic classification.

Conclusions

We experimentally grew and dissolved diamonds compositionally similar to natural lithospheric diamonds; in growth experiments, entrapped inclusions were compositionally similar to those found in natural lithospheric diamonds, although they were not crystalline. The experiments presented here, along with previous ones confirm that all diamonds (monocrystalline, fibrous, polycrystalline, and those formed during high-pressure metamorphism) grow by similar reactions in hydrous carbonate-silicate-rich melts in the mantle. This suggests that their differences are due to different kinetic growth regimes. In our experiments, diamonds underwent dissolution in the absence of graphite, indicating that

natural diamonds can dissolve in the mantle within the same fluids from which they grow, and alternating growth and dissolution episodes do not necessarily require protracted periods. This implies that both diamond growth and dissolution involve redox processes governed by reactions that do not conserve oxygen. Growth involves oxygen production and depends on the ability of the system to recombine this oxygen; diamond growth requires that oxygen sinks be present along with the parental fluids/melts. Such sinks could be graphite or metallic and/or sulphide phases, which are commonly observed as inclusions in natural lithospheric diamonds. Alternating growth and dissolution episodes may also be governed by local redox conditions in the mantle. These processes may not be limited to the lithosphere and may also apply to the sublithospheric mantle.

Diamond growth and dissolution experiments demonstrate that the histories of diamonds in the mantle are governed by complex processes, and that studying natural diamonds requires careful attention and multiple approaches. Particularly, evidence of the occurrence of multiple dissolution events within a single diamond shows that a significant portion of diamonds' histories may be missing, complicating their reconstruction.

Based on our experimental results, we demonstrate that, depending on the growth rate (possibly linked to the amount of water present), diamonds may trap both syngenetic inclusions representing their source medium and protogenetic inclusions that may be totally independent of and much older than the growth medium. In other words, diamonds grow and encapsulate all that surrounds them. No distinction is obvious between these two kinds of inclusions. Therefore, the use of trapped inclusions to date their host diamonds requires careful multi-analytical and structural characterization to prove that they are chemically and isotopically equilibrated, and thus synchronous.

Acknowledgments

We thank the Bayerisches Geoinstitut staff and especially Dan Frost, Ester Posner, and Katherine Armstrong for their always warm welcome, kind help, and support during the experiments performed at BGI Bayreuth. We also thank the Laboratoire Magmas et Volcans staff for their assistance during experiments performed in Clermont-Ferrand. HB acknowledges Jean-Pierre Lorand for donating the lherzolite sample, Pierre Cartigny for very

fruitful discussions, and Robert Dennen for his insightful comments. This manuscript benefited from a previous review from Thomas Stachel. We are grateful to the constructive peer review process handled by Dr Bernard Charlier and provided by Dr Sami Mikhail, Dr Oden Navon and Dr Yaakov Weiss, which improved the clarity of this contribution. The IMPMC FIB and SEM facilities are supported by Région Ile de France Grant SESAME 2006 NOI-07-593/R, INSU-CNRS, INP-CNRS, SU, and by a French National Research Agency (ANR) Grant ANR-07-BLAN-0124-01. This work was supported by the TelluS Program of CNRS-INSU to HB and by Campus France through the PHC PROCOPE 2017 PROJET N° 35376VH to HB.

Appendix A. Supplementary Material

Within this supplementary appendix, the reader can find two tables and height figures.

Table S1 describes the details of the experiments, table S2 summarises raw semi-quantitative EDX analysis of matrix glasses from SEM for growth experiments.

Fig S1 shows a larger view in sample #52 of the glassy piece showing nano-diamonds growing in the hydrous melt quenched as a mingled glass. Fig S2 shows SEM images of the seed milled with FIB which exhibits a rim of inclusions trapped at the interface between the initial surface of the seed and the grown area, sample #53. Fig S3 shows SEM image of diamond growth on seed of sample #53. Fig S4 shows for sample #55 a SEM image of diamond growth on a broken cube made of one type Ia diamond broken anvil. Fig S5 shows for sample #52 a SEM image of spontaneous nucleation and growth of a diamond (1670°C, 6 hours) with octahedral shape. Fig S6 shows for sample #35, a SEM image of the dissolution process at 1450°C 7G GPa, during 5 hours. Fig S7 shows for sample #38 a SEM image of dissolution of a large initial diamond cube (type Ia broken diamond anvil) after 27 hours at 1300-1400°C, 7 GPa. Fig S8 exhibits major oxide variation diagrams of inclusions trapped in diamonds compositions (in wt.%, normalized on a volatile-free basis).

Data Availability

Data are included as supplementary materials, they can also be obtained in the Zenodo open data repository (CERN)

https://doi.org/10.5281/zenodo.10361702

References

Bataleva, Y.V., Palyanov, Y.N., Sokol, A.G., Borzdov, Y.M., Palyanova, G.A. (2012) Conditions for the origin of oxidized carbonate–silicate melts: Implications for mantle metasomatism and diamond formation. Lithos 128–131, 113–125.

Bataleva, Y.V., Palyanov, Y.N., Borzdov, Y.M., Kupriyakov, I.N., Sokol, A.G. (2016) Synthesis of diamonds with mineral, fluid and melt inclusions. Lithos 265, 292–303.

Bezmen, N.I., Gorbachev, P.N., Shalynin, A.I. (2006) Platinum solubility in water-bearing magnesian basaltic melts at 1200°C and 2 kbar. Dokl. Earth Sci. 406, 122–127.

Blaine, F.A., Linnen, R.L., Holtz, F., Brugmann, G.E. (2005) Platinum solubility in haplobasaltic melt at 1250°C and 0.2 GPa: The effect of water content and oxygen fugacity. Geochim. Cosmochim. Ac. 69, 1265–1273.

Boyd, S.R., Pineau, F., Javoy, M. (1994) Modelling the growth of natural diamonds. Chem. Geol. 116, 29–42.

Bulanova, G.P. (1995) The formation of diamond. J. Geochem. Explor. 53, 1–23.

Bulanova, G.P., Griffin, W.L., Ryan, C.G. (1998) Nucleation environment of diamonds from Yakutian kimberlites. Mineral. Mag. 62, 409–419.

Bulanova, G.P., Wiggers de Vries, D.F., Pearson, D.G., Beard, A., Mikhail, S., Smelov, A.P., Davies, G.R. (2014) An eclogitic diamond from Mir pipe (Yakutia), recording two growth events from different isotopic sources. Chem. Geol. 381, 40-54.

Bureau H., Keppler, H., (1999) Complete miscibility between silicate melts and hydrous fluids in the upper mantle: experimental evidence and geochemical implications. Earth and Planet. Sci. Lett., 165, 187-196.

Bureau, H., Langenhorst, F., Auzende, A.-L., Frost, D.J., Estève, I., Siebert, J. (2012) The growth of fibrous, cloudy and polycrystalline diamonds, Geochim. et Cosmochim. Acta, 77, 202-214.

Bureau, H., Frost, D.J., Bolfan-Casanova, N., Leroy, C., Esteve, I., Cordier P. (2016) Diamond growth in mantle fluids. Lithos 265, 4-15.

Bureau, H., Remusat, L., Esteve, I., Pinti, D., Cartigny, P. (2018) Diamond Growth in Mantle Fluids, Sci. Adv., 4, eaat1602.

Daver, L., Bureau, H., Boulard, E., Gaillou, E., Cartigny, P., Pinti, D., Belhadj, O., Guignot, N., Foy, E., Estève, I., Baptiste, B. (2022) From the lithosphere to the lower mantle: an aqueous-rich metal-bearing growth environment to form type IIb blue diamonds, Chem. Geol. 613, 121163, https://doi.org/10.1016/j.chemgeo.2022.121163.

Deines, P., 1980. The carbon isotopic composition of diamonds: relationship to diamond shape, color, occurrence and vapor composition. Geochim. et Cosmochim. Acta 44, 943-961.

Dvir O. and Kessel R. (2017), The effect of CO2 on the water-saturated solidus of K-poor peridotite between 4 and 6 GPa. Geochimica et Cosmochimica Acta 206: 184-200.

Fagan, AJ, Luth, RW (2011) Growth of diamond in hydrous silicate melts. Contrib. Mineral. Petrol. 161:229–236

Fedortchouk, Y., Chinn, I.L., Kopylova, M.G. (2017) Three styles of diamond resorption in a single kimberlite: effects of volcanic degassing and assimilation. Geology 45, 10, 871-874.

Fedortchouk, Y. (2019) A new approach to understand diamond surface features based on a review of experimental and natural diamond studies. Earth-Sci. Rev. 193, 45-65. https://doi.org/10.1016/j.earscirev.2019.02.013.

Fedortchouk, Y., Liebske, C., McCammon, C (2019). Diamond destruction and growth during mantle metasomatism: an experimental study of diamond resorption features. Earth and Planet. Sci; let. 506, 493-506.

Glinnemann, J., Kusaka, K., Harris, J.W., 2003. Oriented graphite single-crystal inclusions in diamond. Zeitschrift für Kristallographie-Crystalline Materials 218, 733-739.

Gress, M.U., Howell, D., Chinn I.L., Speich, L., Kohn, S.C., van den Heuvel, Q., Shulten, E., Pals, A.S.M., Davies, G.R. (2018) Episodic diamond growth beneath the Kaapvaal Craton at Jwaneng Mine, Bostwana. Miner. and Petrol., 112, S219-S229.

Gress, M.U., Timmerman, S., Chinn, I.L., Koornneef, J.M., Thomassot, E., Van der Valk, E.A.S., Van Zuilen, K., Bouden, N, Davies, G.R. (2021) Two billion years of episodic and simultaneous websteritic and eclogitic diamond formation beneath the Orapa kimberlite cluster, Bostwana. Contrib. Miner. Petrol. 176, 54, https://doi.org/10.1007/s00410-021-01802-8

Griffin, W.L., Jaques, A.L., Sie, S.H., Ryan, C.G., Cousens, D.R., Suter, G.F. (1988) Conditions of diamond growth—A proton microprobe study of inclusions in west Australian diamonds. Contrib. Min. Petrol. 99:143–158

Grove T. (1981) Use of FePt alloys to eliminate the iron loss problem in 1atmosphere gas mixing experiments: theoretical and practical considerations. Contrib. Miner. Petrol. 78, 298-304.

Gurney, J.J., Hildebrand, P.R., Carlson, J.A., Fedortchouk, Y., Dyck, D.R., (2004). The morphological characteristics of diamonds from the Ekati property, Northwest Territories, Canada. Lithos 77, 21–38.Huang, F., Sverjensky, D.A. (2020) Mixing of carbonatitic into saline fluid during panda diamond formation. Geochimica et Cosmochimica Acta, 284, 1-20.

Harris, J.W., Smit, K.V., Fedortchouk, Y., Moore, M. (2022) Morphology of Monocrystalline Diamond and its Inclusions. Rev. in Miner. & Geochem., Vol. 88 pp. 119-166.

Harrison, E.R., Tolansky, S. (1964). Growth history of a natural octahedral diamond. Proceedings of The Royal Society A 279, 1379.

Jablon, B.M., Navon, O. (2016). Most diamonds were created equal. Earth and Planet. Sci. Lett. 443, 41-47.

Jacob, D.E., Dobrzhinetskaya, L., With, R. (2014) New insight into polycristalline diamond genesis from modern nanoanalytical techniques. Earth Sci. Rev., 136, 21-35.

Kessel R., Ulmer P., Pettke T. and Schmidt M. W. (2005b) The water-basalt system at 4 to 6 GPa: phase relations and second critical endpoint in a K-free eclogite at 700 to 1400 C. Earth Planet. Sci. Lett. 237, 873–892

Kiseeva, E.S., Litasov, K.D., Yaxley, G.M., Ohtani, E., Kamenetsky, V.S. (2013) Melting and phase relations of carbonated eclogite at 9–21 GPa and the petrogenesis of alkali-rich melts in the deep mantle. J. Petrol. 54:1555–1583

Keppler H. and Frost D. J. (2005) Introduction to minerals under extreme conditions. In Mineral Behaviour at Extreme Conditions (ed. R. Miletich). EMU Notes in Miner., pp. 1–30.

Klein-BenDavid O., Izraeli, E.S., Hauri, E., Navon O. (2004) Mantle fluid evolution – a tale of one diamond. Lithos, 77, 243-253.

Klein-BenDavid O., Pearson D.G., Nowell G.M., Ottley C., McNeill J.C.R., Cartigny P. (2010) Mixed fluid sources involved in diamond growth constrained by Sr–Nd–Pb–C–N isotopes and trace elements. Earth and Planet. Sci. let. 289, 123–133.

Khokhryakov, A.F, Pal'yanov, Y.N. (2007) The evolution of diamond morphology in the process of dissolution: Experimental data. Am. Mineral., 92, 909-917.

Khokhryakov, A.F., Pal'yanov, Y.N. (2010). Influence of the fluid composition on diamond dissolution formsin carbonate melts. Am. Mineral. 95, 1508-1514.

Khokhryakov, A.F., Pal'yanov, Y.N. (2015) Effect of crystal defect on diamond morphology during dissolution in the mantle. Am. Miner. 100, 1528-1532. http://dx.doi.org/10.2138/am-2015-5131

Koornneef, J.M., Gress, M.U., Chinn, I.L., Jesma, H.A., Harris, J.W., Davies, G.R. (2017) Archean and Proterozoic diamond growth from contrasting styles of large-scale magmatism. Nat. Comm. DOI:10.1038/s41467-017-00564-x

Litasov KD, Shatskiy A, Ohtani E (2014) Melting and subsolidus phase relations in peridotite and eclogite systems with reduced COH fluid at 3–16 GPa. Earth Planet. Sci. Lett 391:87–99

Lorand, J.P., Luguet, A., Alard, O., Bezos, A., Meisel, T. (2008) Adundance and distribution of platinum-group elements in orogenic lherzolites; a case study in a Fontete Rouge lherzolite –French Pyrénées). Chem. Geol. 248, 174-194.

Luth, R.W., Palyanov, Y.N., Bureau, H. (2022) Experimental Petrology Applied to Natural Diamond Growth. Rev. in Mineral. & Geochem., Vol. 88 pp. 755-802

Mikhail, S., Rinaldi, M., Mare, E.R., Sverjensky, D.A. (2021) A genetic metasomatic link between eclogitic and peridotitic diamond inclusions. Geochemical Perspectives Letters 17, 33-38.

Navon, O., Hutcheon I.D., Rossman, G.R., Wasserburg, G.J. (1988) Mantle-derived fluids in diamond micro-inclusions. Nature 335, 784-789.

Nestola, F., Jung, H., Taylor, L.A. (2017) Mineral inclusions in diamonds may be synchronous but not syngenetic. Nat. Comm. DOI: 10.1038/ncomms14168

Nestola, F. Jacob, D.E., Pamato, M.G., Pasqualetto, L., Oliveira, B., Greene, S., Perritt, S., Chinn, I., Milani, S., Kueter, N., Sgreva, N., Nimis, P., Secco, L., Harris, J.W. (2019) Protogenetic inclusions and the age of diamonds. Geology https://doi.org/10.1130/G45781.1.

Nimis, P., Alvar, M., Nestola, N., Angel, R.J., Marquart, K., Rustioni, G., Harris, J.W., Marone F. (2016) First evidence of hydrous silicic fluid films around solid inclusions in gem-quality diamonds. Lithos 260, 384-389.

Pal'yanov Y.N., Sokol A.G., Bozdov Y.M., Khokhryakov A.F., Sobolev N.V., (1999). Diamond formation from mantle carbonate fluids. Nature 400, 417–418.

Pal'yanov Y.N., Sokol A.G. (2009) The effect of composition of mantle fluids/melts on diamond formation processes. Lithos 1125, 690-700, Pal'yanov Y.N., Bataleva, Y.V., Sokol, A.G., Borzdov, Y.M., Kupriyanov, I.N., Reutsky, V.D., Sobolev, N.V. (2013) Mantle-slab interaction and redox mechanism of diamond formation. Proc. of the Nat. Acad. of Sci. 110.

Palyanov YN, Sokol AG, Khokhryakov AF, Kruk AN (2015) Conditions of diamond crystallization in kimberlitemelt: experimental data. Russ. Geol. Geophys. 56:196–210

Palyanov, Y.N., Borzdov, Y.M., Sokol, A.G., Bataleva, Y.V., Kupriyanov, I.N., Reutsky, V.N., Wiedenbeck, M., Sobolev, N.V. (2021) Diamond formation in an electric field under deep Earth conditions. Sci. Adv. 7:eabb4644

Pearson, D.G., Shirey, S.B., Harris, J.W., Carlson, R.W. (1998). Sulphide inclusions in diamonds from the Koffiefontein kimberlite, S Africa: constraints on diamond ages and mantle Re–Os systematics. Earth and Planetary Sciences Letters, 160, 311-326.

Rinaldi, M. Mikhail, S., Sverjensky, D.A., Kalita, J. (2023) The importance of carbon to the formation and composition of silicates during mantle metasomatism. Geochimica et Cosmochimica Acta, 356, 105-115.

Robinson, D.N., 1979. Surface Textures and Other Features of Diamonds. The University of Cape Town, Cape Town, pp. 221 (Ph.D. thesis).

Shirey, S.B., Pearson, D.G., Walter, M.J., Aulbach, S., Brenker, F.E., Bureau, H., Burnham, A.D., Cartigny, P., Chacko, T., Frost, D.J., Hauri, E.H., Jacob, D.E., Jacobsen, S.D., Kohn, S.C., Luth, R.W., Mikhail, S., Navon, O., Nestola, F., Nimis, P., Smit, K.V., Smith, E.N., Stachel, T., Stagno, V., Steele, A., Thomassot, E., Thomson, A.R., Weiss, Y. (2019). Diamonds and the Mantle Geodynamics of Carbon: Deep Mantle Carbon Evolution from the Diamond Record. In Orcutt, B., Daniel, I., and Dasgupta, R. (Eds.) Deep Carbon: Past to Present. Cambridge University Press.

Shiryaev, A.A., Zubavichus, Y.V., Veligzhanin, A.A., McCammon, C., 2010. Local environment and valence state of iron microinclusions in fibrous diamonds: X-Ray Absorption and Mössbauer data. Russ. Geol. and Geophys., 2010, 51(12), pp. 1262–1266, Nature Precedings

Smart, K. A., Tappe, S., Stern R.A., Webb, S.J., Ashwal, L.D. (2016) Early Archean tectonics and mantle redox recorded in Witwatersand diamonds. Nature Geoscience volume 9, pages 255–259 (2016)

Smit, K.V., Shirey, S.B., Stern R.A., Steele A., Wang, W. (2016). Diamond growth from C–H–N–O recycled fluids in the lithosphere: Evidence from CH_4 micro-inclusions and $\delta^{13}C$–$\delta^{15}N$–N content in Marange mixed-habit diamonds. Lithos 265, 68-81.

Smit, K.V., Timmernann, S., Aulbach, S. Shirey, S.B., Richardson, S.H., Phillips, D., Pearson, G. (2022). Geochronology of Diamonds. Rev. in Mineral. & Geochem. Vol. 88 pp. 567-636.

Sokol A.G., Pal'yanov Y.N. (2008) Diamond formation in the system MgO-SiO2-H2O-C at 7.5 GPa and 1600°C. Contrib. Mineral. Petrol., 155, 33-43.

Sokol, A.G., Palyanova G.A., Palyanov, Y.N., Tomilenko, A.A., Melenevsky, V.N. (2009) Fluid regime and diamond formation in the reduced mantle: Experimental constraints. Geochim. et Cosmochim. Acta 73, 5820–5834.

Sokol A.G., Tomilenko A.A., Palyanova, G.A., Pal'yanov Y.N., Sobolev, N.V. (2017) Stability of methane in reduced C-O-H fluid at 6.3 GPa and 1300-1400°C. Doklady Earth Sci. Vol. 474, Part 2, pp. 680–683.

Stachel, T., Harris, J.W., Brey, G.P. (1988) Rare and unusual mineral inclusions in diamonds from Mwadui, Tanzania. Contrib. Mineral. Petrol. 132, 34-47.

Stachel, T., Luth R.W. (2015) Diamond formation – Where, when and how? Lithos 220-223, 200-220.

Stachel, T., Chacko, T., R.W., Luth (2017) Carbon isotope fractionation during diamond growth in depleted peridotite: Counterintuitive insights from modelling water-maximum CHO fluids as multi-component systems. Earth and Planet. Sci. Lett. 743, 44-51.

Stachel, T., Aulbach, S., Harris, J.W. (2022) Mineral Inclusions in Lithospheric Diamonds, Rev. in Miner. & Geochem., Vol. 88 pp. 307-392

Stagno, V., Frost, D.J. (2010) Carbon speciation in the asthenosphere: experimental measurements of the redox conditions at which carbonate bearing melts coexist with graphite or diamond in peridotite assemblages. Earth Planet. Sci. Lett. 300, 72–84.

Stagno V, Ojwang DO, McCammon CA, Frost DJ (2013) The oxidation state of the mantle and the extraction of carbon from Earth's interior. Nature 493:84–88

Sunagawa I., (1984) Morphology of natural and synthetic diamond crystals. Materials science of the Earth's interior In terra Scientific Publishing, Tokyo, Japan, pp. 303-330.

Sverjensky, D.A., Stagno, V., Huang, F. (2015) Important role for organic carbon in subduction-zone fluids in the deep carbon cycle. Nature Geoscience, 7, 909-913.

Thomassot, E., Cartigny, P., Harris, J.W., Lorand, J.P., Rollion-Bard, C., Chaussidon M. (2009) Metasomatic diamond growth: A multi-isotope study (C^{13}, N^{15}, S^{33}, S^{34}) of sulphide inclusions and their host diamonds from Jwaneng (Botswana) Earth and Planet. Sci. Lett., 282, 79-90, DOI10.1016/j.epsl.2009.03.001.

Viljoen, K.S., Swash, P.M., Otter, M.L., Schulze, D.J., Lawless, P.J. (1992) Diamondiferous garnet harzburgites from the Finsch kimberlite, Northern Cape, South Africa. Contrib. Mineral. Petrol. 110, 133-138.

Wang, W. (1998) Formation of diamond with mineral inclusions of ‘’mixed’’ eclogite and peridotite paragenesis. Earth Planet. Sci. Lett. 160:831–843

Weiss Y., Kessel R., Griffin W.L., Kiflawi I., Klein-BenDavid O., Bell D.R., Harris J.W., Navon O. (2009) A new model for the evolution of diamond-forming fluids: Evidence from microinclusion-bearing diamonds from Kankan, Guinea, Lithos, **112S**, 660-674.

Weiss, Y., McNeill, J., Pearson, G., Nowell, G.M., Ottley, G.J (2015) Highly saline fluids from a subducting slab as the source for fluid-rich diamonds. Nature 524, 339–342. .

Weiss, Y., Czas, J., Navon, O. (2022) Fluid inclusions in fibrous diamonds. Reviews in Mineralogy & Geochemistry Vol. 88 pp. 475-532.Wyllie P.J., Ryabchikov I.D. (2000) Volatile components, magmas, and critical fluids in upwelling mantle. J. of Petrol., **41**, 1195-1206.

Wyllie, P. J. and Ryabchikov, I.D. (2000) Volatile Components, Magmas, and Critical Fluids in Upwelling Mantle. J. of Petrol., 41, 1195-1206.

Zedgenizov, D.A., Kagi, H., Shatsky, V.S., Ragozin, A.L. (2014) Local variations of carbon isotope composition in diamonds from Sao-Luis (Brazil): Evidence for heterogeneous carbon reservoir in sublithospheric mantle. Chem. Geol. 363, 114-124.

Figure Captions

Figure 1

A. Optical photograph of diamond pieces from broken diamond anvils; scale is 1 mm. **B.** SEM image of one diamond seed oxidized in air at 1000 °C for 10 minutes; scale is 10 µm. **C.** Open capsule of sample #53 during loading, showing the peridotite sphere in carbonate powder (seeds, graphite, and water are below); scale is 1 mm. **D.** Open capsule of sample #53 after the run. The fluid was lost upon opening, the round, yellow central part is mainly composed of seeds, the dark green elongated area is a peridotite (LHERZ) glassy layer, and the surrounding white powder is mostly carbonate. The scale bar is 1 mm.

Figure 2

SEM images showing diamond growth at 7 GPa. Seeds are covered with tiny carbonate crystals agglomerated in clusters. **A.** Sample #51 (1430 °C, 6 hours), showing growth on seeds. **B.** Sample #52 (1670 °C, 6 hours), showing massive growth on the seeds and new diamond crystals attached to seed growths. **C.** Sample #52, showing an octahedral diamond that spontaneously nucleated and grew. **D.** Sample #53 (1400 °C, 24 hours), showing growth on seeds. **E.** Sample #54 (1400 °C, 24 hours), showing an octahedral diamond that spontaneously nucleated and grew. **F.** Sample #55 (1400 °C, 6 hours), showing growth on seeds.

Figure 3

SEM images of sample #52. **A.** A large glassy phase is highly and heterogenously vesiculated and surrounded by white carbonates. This vermicular texture suggests that a supercritical fluid developed immiscibility during quenching. **B.** Enlarged view of the lower area of this glassy phase, exhibiting small octahedral diamond crystals ("nano-diamonds") in the process of formation just after nucleation in the single supercritical phase. A larger diamond with growth textures is visible just below this area, and small, white carbonate aggregates are above.

Figure 4

SEM images of diamonds that trapped inclusions during experimental growth (top) before and (middle, bottom) after FIB milling. **A–C.** Sample #53-1. Exposed inclusions are aligned on the initial surface of the seed, marked by the white dashed line in **B**. Different kinds of inclusions are exposed: mixed glasses with vesicles, and bulk white platinum inclusions (Pt, red arrows in **B**). Red crosses correspond to chemical analyses in Table 4. **D–F.** Sample #52-9. Inclusions are melt (now glass) or fluid (now empty voids). **G–I.** Sample #52-5. A large glassy inclusion terminates with an empty void that was initially filled with aqueous fluid. **J–L.** Sample #53-6. Massive growth occurred on the top of the seed diamond, and inclusions are aligned along the initial surface of the seed.

Figure 5

SEM images of samples from dissolution experiments. **A.** Sample #32, 1450 °C, 6 hours. Seeds are transformed and exhibit laminations. **B.** Sample #35, 1450 °C, 5 hours. Seeds exhibit advanced lamination. **C.** Sample #35. A large cube of broken diamond that was dissolved and rounded, and no longer shows a clear trigonal shape. **D.** Sample #38, 1300–1400 °C, 27 hours. Seeds are completely foliated. **E.** Sample #38. The surface of a large

initial diamond cube is etched and partly dissolved, forming stepped crystal surfaces. **F.** Sample #38. A large, resorbed diamond cube with a rounded final shape that exhibits trigonal and square pits. **G.** Sample #45, 1350 °C, 6 hours. Seeds are partly dissolved. **H.** Sample #44, 1350 °C, 6 hours. Seeds are partly dissolved and show pits. **I.** Sample #49, 1400 °C, 6 hours. A partly dissolved cube now showing a cuboctahedral shape, typical of crystal rounding via mantle resorption.

Figure 6

The compositions of solid diamond inclusions (blue stars) and matrix glasses (red spots) from our experiments plot within the global compositional range of high-density fluids trapped in natural fibrous diamonds (grey shaded area; after Weiss et al., 2015 and references therein).

Figures

Figure 1

A. Optical photograph of diamond pieces from broken diamond anvils; scale is 1 mm. **B.** SEM image of one diamond seed oxidized in air at 1000 °C for 10 minutes; scale is 10 µm. **C.** Open capsule of sample #53 during loading, showing the peridotite sphere in carbonate powder (seeds, graphite, and water are below); scale is 1 mm. **D.** Open capsule of sample #53 after the run. The fluid was lost upon opening, the round, yellow central part is mainly composed of seeds, the dark green elongated area is a peridotite (LHERZ) glassy layer, and

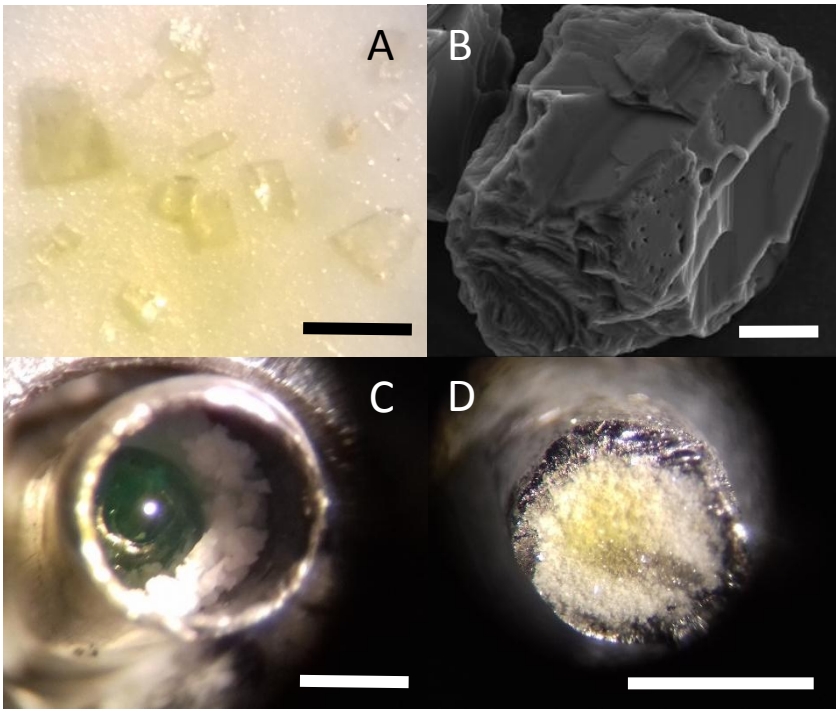

the surrounding white powder is mostly carbonate. The scale bar is 1 mm.

Figure 2

SEM images showing diamond growth at 7 GPa. Seeds are covered with tiny carbonate crystals agglomerated in clusters. **A.** Sample #51 (1430 °C, 6 hours), showing growth on seeds. **B.** Sample #52 (1670 °C, 6 hours), showing massive growth on the seeds and new diamond crystals attached to seed growths. **C.** Sample #52, showing an octahedral diamond that spontaneously nucleated and grew. **D.** Sample #53 (1400 °C, 24 hours), showing growth on seeds. **E.** Sample #54 (1400 °C, 24 hours), showing an octahedral diamond that spontaneously nucleated and grew. **F.** Sample #55 (1400 °C, 6 hours), showing growth on seeds.

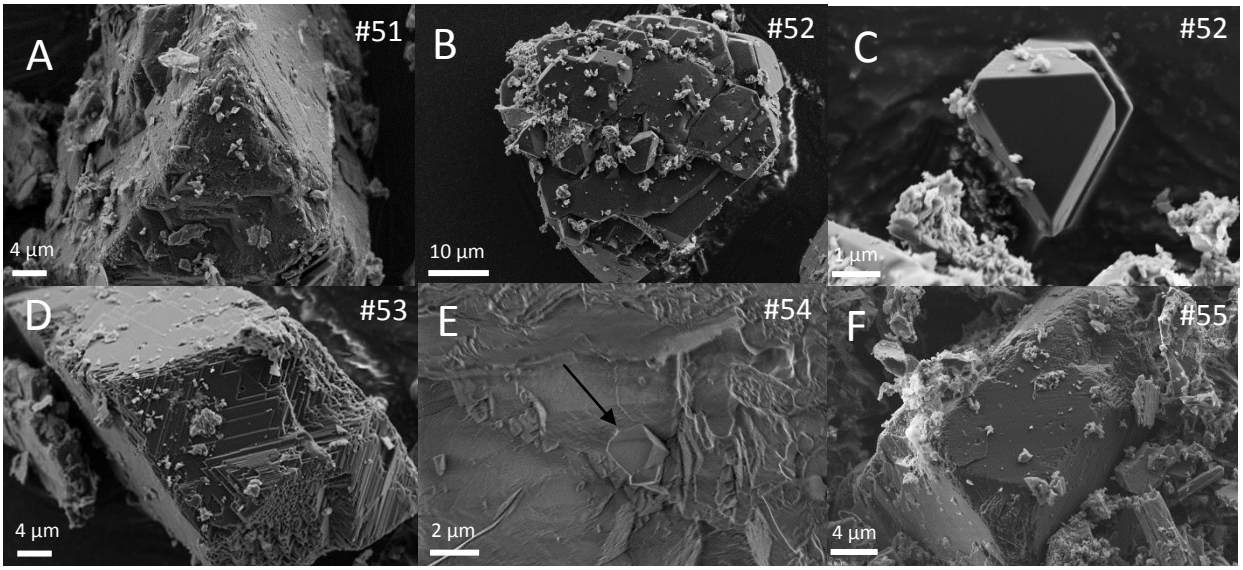

Figure 3

SEM images of sample #52. **A.** A large glassy phase is highly and heterogenously vesiculated and surrounded by white carbonates. This vermicular texture suggests that a supercritical fluid developed immiscibility during quenching. **B.** Enlarged view of the lower area of this glassy phase, exhibiting small octahedral diamond crystals ("nano-diamonds") in the process of formation just after nucleation in the single supercritical phase. A larger diamond with growth textures is visible just below this area, and small, white carbonate aggregates are above.

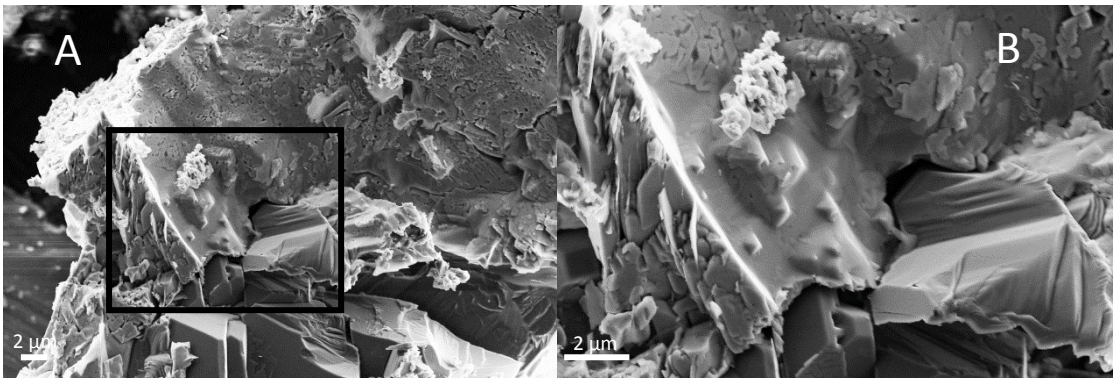

928

Figure 4

SEM images of diamonds that trapped inclusions during experimental growth (top) before and (middle, bottom) after FIB milling. **A–C.** Sample #53-1. Exposed inclusions are aligned on the initial surface of the seed, marked by the white dashed line in **B**. Different kinds of inclusions are exposed: mixed glasses with vesicles, and bulk white platinum inclusions (Pt, red arrows in **B**). Red crosses correspond to chemical analyses in Table 4. **D–F.** Sample #52-9. Inclusions are melt (now glass) or fluid (now empty voids). **G–I.** Sample #52-5. A large glassy inclusion terminates with an empty void that was initially filled with aqueous fluid. **J–L.** Sample #53-6. Massive growth occurred on the top of the seed diamond, and inclusions are aligned along the initial surface of the seed.

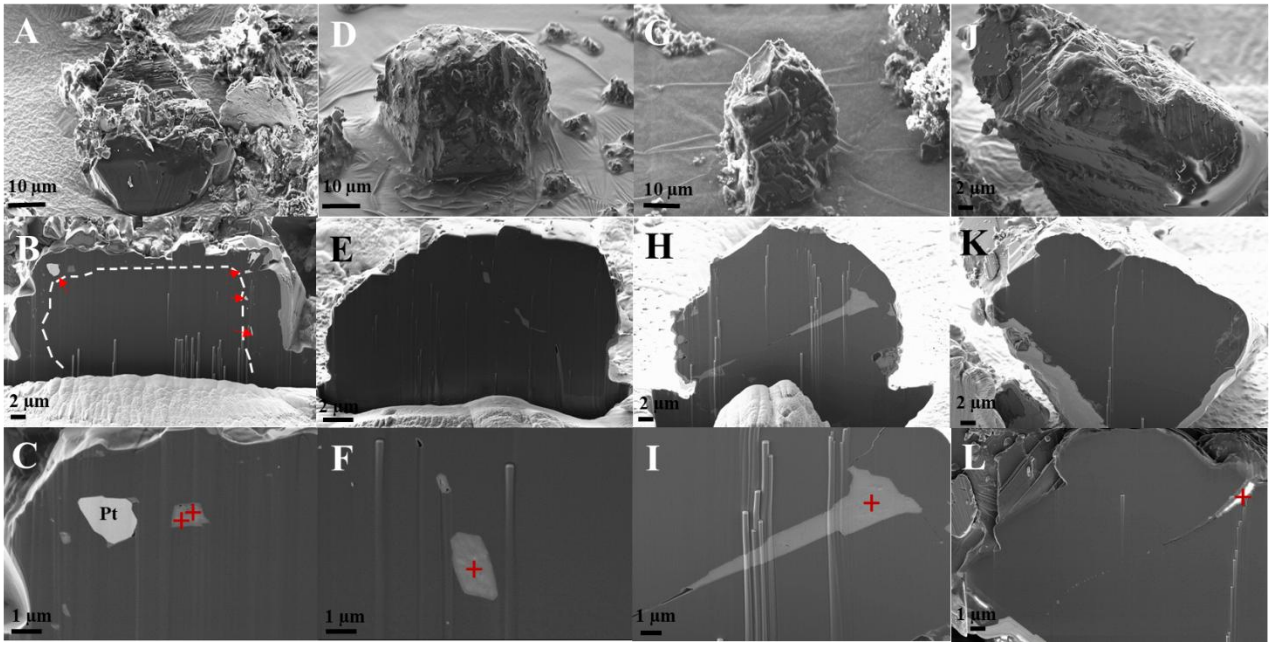

940 **Figure 5**

941 SEM images of samples from dissolution experiments. **A.** Sample #32, 1450 °C, 6 hours.
942 Seeds are transformed and exhibit laminations. **B.** Sample #35, 1450 °C, 5 hours. Seeds
943 exhibit advanced lamination. **C.** Sample #35. A large cube of broken diamond that was
944 dissolved and rounded, and no longer shows a clear trigonal shape. **D.** Sample #38, 1300–
945 1400 °C, 27 hours. Seeds are completely foliated. **E.** Sample #38. The surface of a large
946 initial diamond cube is etched and partly dissolved, forming stepped crystal surfaces. **F.**
947 Sample #38. A large, resorbed diamond cube with a rounded final shape that exhibits trigonal
948 and square pits. **G.** Sample #45, 1350 °C, 6 hours. Seeds are partly dissolved. **H.** Sample #44,
949 1350 °C, 6 hours. Seeds are partly dissolved and show pits. **I.** Sample #49, 1400 °C, 6 hours.
950 A partly dissolved cube now showing a cuboctahedral shape, typical of crystal rounding via
951 resorption.

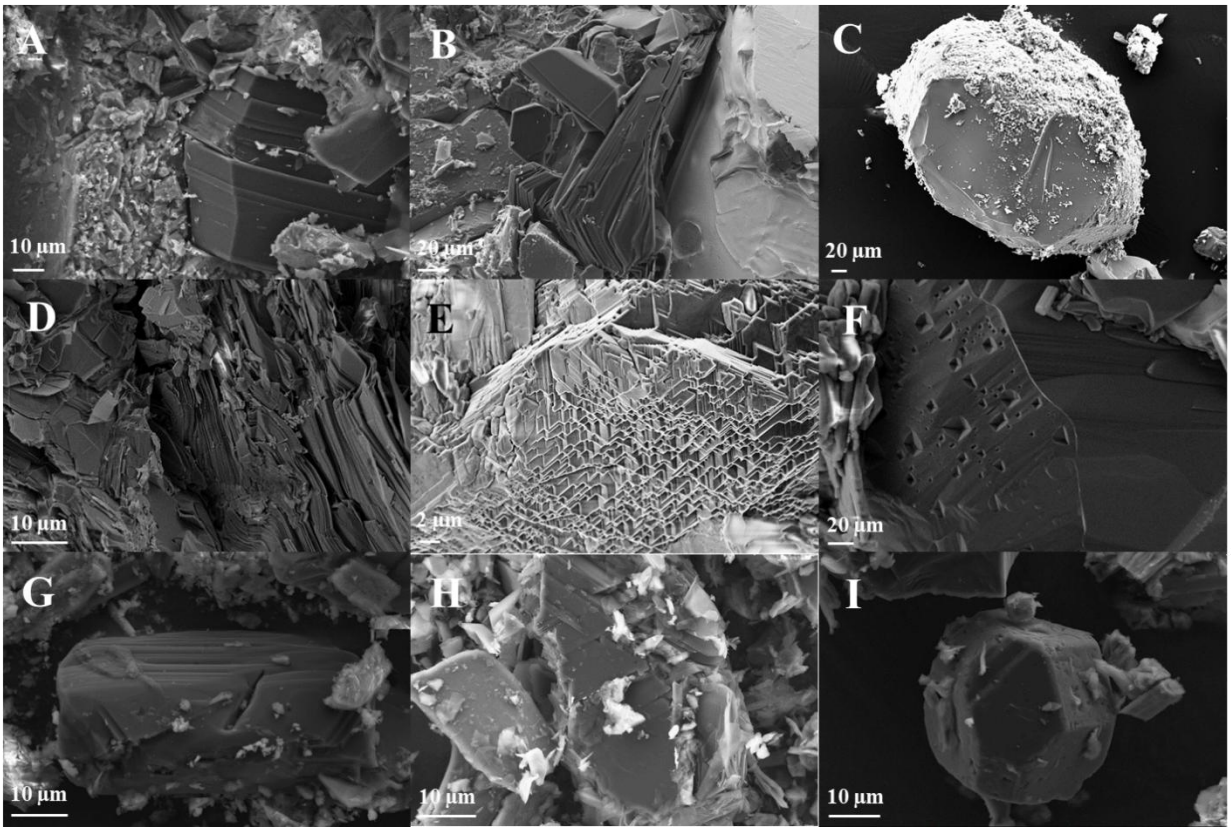

952

Figure 6

The compositions of solid diamond inclusions (blue stars) and matrix glasses (red spots) from our experiments plot within the global compositional range of high-density fluids trapped in natural fibrous diamonds (grey shaded area; after Weiss et al., 2015 and references therein).

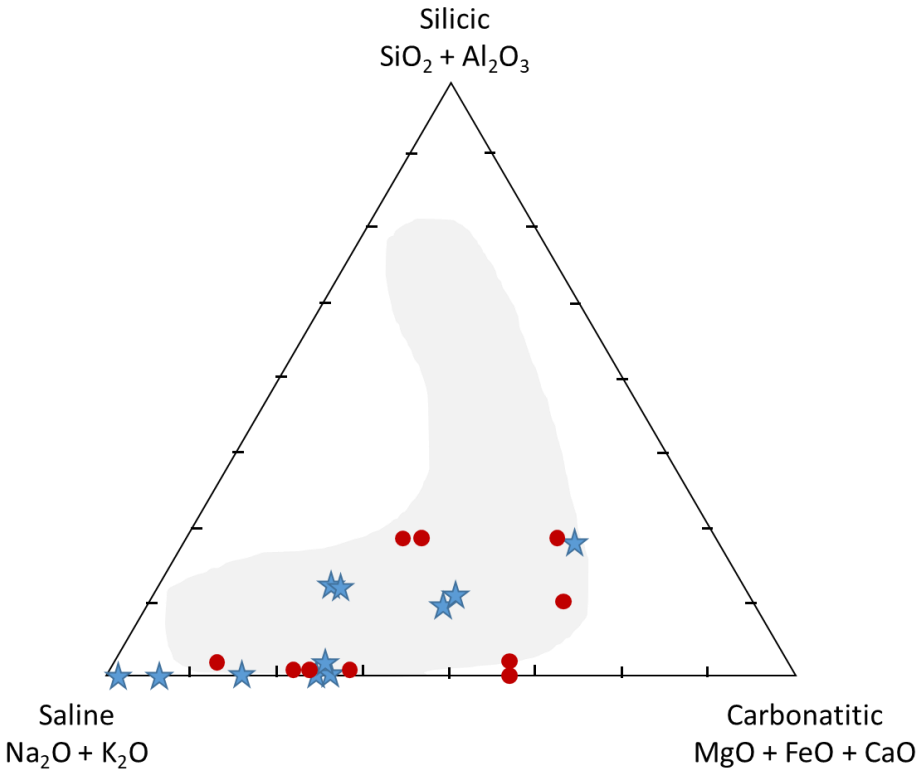

960 **Table 1**: starting materials

Name	Description	Composition
MORB	Powder of Natural mid-ocean-ridge-basalt, Indian ridge*	DRX analysis: 38.26% $CaAl_2Si_2O_8$ 13.25% $(Mg_{1.41}Fe_{0.59})\ SiO_4$ 44.72% $(Ca_{0.8}Mg_{1.2})Si_2O_6$
R_LHERZ	Powder of Natural lherzolith FONB93 from French Pyrénées**	49% olivine ($Fo_{89.9}$), 33% orthopyroxene (En_{89}–Fs_{10}–Wo_1), 15% Al-rich clinopyroxene ($En_{4.3}$–$Fs_{47.4}$–$Wo_{48.3}$) 3% Al-rich spinel (Cr/Cr+Al=0.092) In wt.%: SiO_2 43.26; Al_2O_3 3.23; Fe_2O_3T 8.32; MnO 0.12; MgO 37.90; CaO 3.18; Na_2O 0.27; K_2O 0.002; TiO_2 0.12
G_LHERZ	Glass of natural lherzolith	In wt%.: SiO_2 42.7; Al_2O_3 2.29; Fe_2O_3T 8.26; MgO 39.3; CaO 4.4; Na_2O 0.5
Graphite	Powder	C
Ca carbonate	Powder	$CaCO_3$
Na carbonate	Powder	Na_2CO_3
K carbonate	Powder	K_2CO_3
Seeds	Powder of commercial diamond seeds, 40-60 µm	C

961 *Bureau et al., 2016

962 ** Lorand et al., 2008

963

964

965 **Table 2a:** Summary of the experiments performed at 7 GPa and results to grow diamonds

Exp.	**Starting materials**	**T°C**	**Time h**	**Starting H_2O/CO_2**	**Results (process and products)**
Growth					
#51	H_2O, Dox, R-LHER K_2CO_3	1430	6	1.8	Aqueous fluid, glass, Carbonates, G, D growth on seeds
#52	H_2O, Dox, C, R-LHERZ, G, $CaCO_3$	1670	6	2.8	Aqueous fluid, glass, Carbonates, seeds, G, spontaneous D growth, growth on seeds
#53	H_2O, Dox, G, C, G-LHERZ, $CaCO_3$, Na_2CO_3, K_2CO_3	1400	24	4.8	Aqueous fluid, glass, Carbonates, seeds, G, D growth on seeds
#54	H_2O, G, C, G-LHEF $CaCO_3$, Na_2CO_3, K_2CO_3	1400	24	4.1	Aqueous fluid, glass, Carbonates, G, D growth on broken cubes, spontaneous D growth
#55	H_2O, Dox, G, C, G-LHERZ, Na_2CO_3	1400	6	4.2	Aqueous fluid, glass, Carbonates, seeds, G, D growth on seeds
#50	H_2O, Dox, C, G, R-LHERZ, Na_2CO_3	1673	6	4.2	Water leak, no fluid, glass, Carbonates, seeds, G, no D growth
#210*	H_2O-NaCl, Dox, G MORB + Natural $CaCO_3$	1350	6		Aqueous fluid, glass, G, Carbonates. Slight D growth on seeds and spontaneous D growth

966 Notations: Exp. Experiment; Dox oxidized diamond seeds; G graphite; MORB Mid Ocean
967 Ridge Basalt; R-LHERZ powder of lherzolith; G-LHERZ glass of lherzolith; C diamond
968 cubic pieces (100-200µm). * from Bureau et al., 2016. (H_2O/CO_2) ratio by weight, graphite
969 not included. In the case of runs #52 and #50 performed at HT, the ratio may reach 0.8 and
970 0.5 assuming all G is dissolved in the fluid. As G is observed in the quenched products, the
971 ratio is higher.

972

Table 2b: Summary of the experiments performed at 7 GPa and results to dissolve diamonds

Exp.	Starting materials	T°C	Time h	Starting H_2O/CO_2	Results (process and products)
Dissolution					
#31	H_2O, Dox, R-LHEI $CaCO_3$, Na_2CO_3 K_2CO_3	1450	6	4.3	Aqueous fluid, Carbonates, glass, resorbed seeds
#32	H_2O, Dox, R-LHEI $CaCO_3$, Na_2CO_3 K_2CO_3	1450	6	2.2	Aqueous fluid, Carbonates, glass, resorbed seeds
#35	H_2O, Dox, C, MOF $CaCO_3$, Na_2CO_3 K_2CO_3	1450	5	1.6	Aqueous fluid, Carbonates, glass, resorbed seeds Resorption of the D cubes
#38	H_2O, Dox, C, MOF $CaCO_3$, Na_2CO_3 K_2CO_3	1300-1400	27	3.2	Aqueous fluid, Carbonates, glass, resorbed seeds Resorption of the D cubes
#44	H_2O, Dox, R-LHEI K_2CO_3	1350	6	4.1	Aqueous fluid, Carbonates, glass, resorbed seeds
#45	H_2O, Dox, R-LHEI $CaCO_3$	1350	6	3.8	Aqueous fluid, Carbonates, glass, resorbed seeds
#49	H_2O, Dox, C, R-LHERZ, Na_2CO_3	1400	6	7.6	Aqueous fluid, Carbonates, glass, resorbed seeds

Notations: Exp. Experiment; Dox oxidized diamond seeds; G graphite; MORB Mid Ocean Ridge Basalt; R-LHERZ powder of lherzolith; G-LHERZ glass of lherzolith; C diamond cubic pieces (100-200µm). * from Bureau et al., 2016. (H_2O/CO_2) ratio by weight, graphite not included. In the case of runs #52 and #50 performed at HT, the ratio may reach 0.8 and 0.5 assuming all G is dissolved in the fluid. As G is observed in the quenched products, the ratio is higher.

Table 3a: Some semi-quantitative SEM-EDX representative analysis of the matrix glasses associated to the seeds for samples #54, #53 and #55 (diamond growth). A strong heterogeneity of carbon is observed, this is due to the strong contamination due to the diamond crystals present close to or below the small pieces of glasses. Raw compositions are presented in Table S2, they show that the total is ranging from 64 to 100. Water is omitted because water cannot be analysed with SEM and because of the strong uncertainties of CO_2 contents, a calculation of water contents by difference to 100 is not possible. Compositions are calculated to obtain a total of 100 wt%. The strong enrichment in Na for sample #55 reflects the fact that only $NaCO_3$ was added for this experiment. Same remark for sample #52 and $CaCO_3$. For samples #54, #53, the 3 carbonates were present. For sample #52, one analysis is performed in a glassy area exhibiting nano-diamonds and vermiculates that witness a strong water degassing during the quench (Figure 3), the four last analyses are performed in the same glassy area.

Growth	#54 GoS	#54 GoS	#53 GoS	#53 C G	#53 GoS	#53 GoS	#55 GoS	#55 G	#52 GoS	#52 GnD	#52 vG	#52 vG	#52 vG
SiO_2	26.68	23.52	12.35	0.45	36.30	23.57	20.89	7.18	8.98	12.03	13.91	18.92	4.95
Al_2O_3	7.60	1.10	2.79	0.00	2.49	3.84	1.75	0.86	0.00	1.03	1.08	1.70	0.55
Na_2O	5.06	3.46	0.74	7.93	1.60	2.64	3.91	18.55	0.00	0.00	0.00	0.00	0.40
MgO	19.43	16.43	9.32	3.21	16.34	13.68	11.60	10.83	4.51	12.99	13.14	14.53	16.23
K_2O	12.63	2.47	5.84	15.13	2.37	12.71	0.00	0.00	0.00	0.00	0.00	0.00	0.00
CaO	0.71	5.67	0.00	6.68	8.94	1.09	0.25	1.66	31.82	22.53	20.30	22.19	16.23
CO_2	27.89	47.34	68.95	66.60	31.96	42.47	61.59	60.92	54.70	51.14	51.57	42.66	66.77
Total	100.00	100.00	100.00	100.00	100.00	100.00	100.00	100.00	100.00	100.00	100.00	100.00	100.00

997 Table 3b: Some semi-quantitative SEM-EDX representative analysis of the matrix glasses
998 associated to the seeds for samples and #35, #38 (diamond dissolution). Same legend as for
999 Table 3a

Dissolution	#35 G	#35 G	#35 G	#38 G	#38 GoS	#38 G	#38 G	#38 G	#38 G	#38 G	#38 G	#38 G	#38 G
SiO_2	21.29	21.07	0.00	19.99	2.96	31.02	12.11	38.94	2.56	24.70	27.05	10.19	21.29
Al_2O_3	4.09	3.73	0.00	5.65	1.02	8.91	4.77	11.76	1.31	7.85	8.11	4.02	4.09
Na_2O	4.42	3.89	12.83	1.99	0.55	2.39	0.67	2.62	1.72	2.27	1.45	1.52	4.42
MgO	18.94	18.77	16.41	4.65	8.99	6.61	8.19	8.85	23.10	11.35	6.93	9.07	18.94
K_2O	3.32	4.96	6.26	0.00	0.00	0.66	4.31	0.78	0.86	1.51	0.00	1.77	3.32
CaO	13.30	19.09	29.68	8.41	13.29	14.79	2.82	12.63	35.23	11.99	11.05	22.70	13.30
CO_2	34.24	27.98	34.82	59.31	73.20	34.62	66.70	23.54	35.22	39.84	44.57	50.73	34.24
Total	100.00	100.00	100.00	100.00	100.00	100.00	100.00	100.00	100.00	100.00	100.00	100.00	100.00

1000 Notations: G Glass; GoS Glass on Seeds; C G carbonate glass; GnD glass with nano-
1001 diamonds; vG vermiculated glass

Table 4: Volatile-free semi-quantitative analysis of the inclusions trapped in diamond seeds. For these analyses, due to the strong carbon contamination from diamond, carbon is not taken into account. Positions of the analysis are indicated on figure 4 with red crosses. No minerals are trapped, all inclusions are glassy, for #53 (1 and 2) the inclusion is highly vesiculated.

	#53-1 1	**#53-1 2**	**#53-6 3**	**#52-5 4**	**#52-9 5**
SiO_2	37.60	23.20	47.35	19.82	30.74
Al_2O_3	6.81	3.74	9.28	0.00	0.00
Na_2O	0.00	0.00	0.00	0.00	0.00
MgO	35.44	44.08	20.98	9.94	12.89
K_2O	13.28	14.74	22.39	0.00	1.59
CaO	6.87	14.23	0.00	70.24	54.79
Total	100.00	100.00	100.00	100.00	100.00

1008